ChemComm

Accepted Manuscript

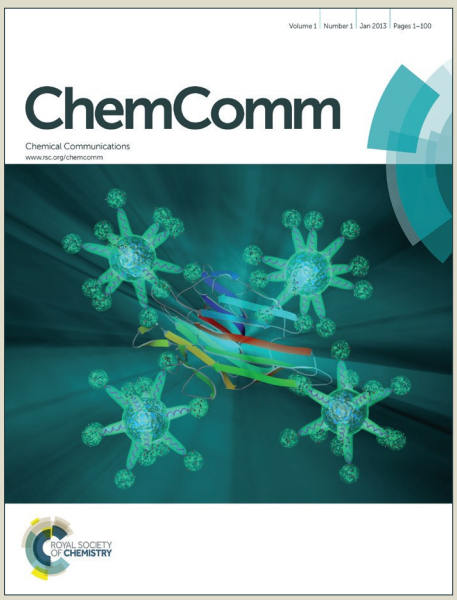

This is an *Accepted Manuscript*, which has been through the Royal Society of Chemistry peer review process and has been accepted for publication.

Accepted Manuscripts are published online shortly after acceptance, before technical editing, formatting and proof reading. Using this free service, authors can make their results available to the community, in citable form, before we publish the edited article. We will replace this *Accepted Manuscript* with the edited and formatted *Advance Article* as soon as it is available.

You can find more information about *Accepted Manuscripts* in the Information for Authors.

Please note that technical editing may introduce minor changes to the text and/or graphics, which may alter content. The journal's standard Terms & Conditions and the Ethical guidelines still apply. In no event shall the Royal Society of Chemistry be held responsible for any errors or omissions in this *Accepted Manuscript* or any consequences arising from the use of any information it contains.

ROYAL SOCIETY OF CHEMISTRY

www.rsc.org/chemcomm

Please do not adjust margins

Chemical Communications

COMMUNICATION

The magnetic and crystal structures of $Sr_{1-\delta}FeO_{2-x}F_x$, a new oxyfluoride

Received 00th January 20xx,
Accepted 00th January 20xx

DOI: 10.1039/x0xx00000x

www.rsc.org/

Bing Li,[a] John Woods,[a] Joan Siewenie,[b] Hien-Yoong Hah,[c,d] Jacqueline A. Johnson,[c,d] Charles E. Johnson,[d] and Despina Louca[a,†]

A new quasi-two-dimensional oxyfluoride, $Sr_{1-\delta}FeO_{2-x}F_x$, has been successfully synthesized by combining topotactic fluoridation and CaH_2 reduction. The introduction of F through this synthesis provides a new route to introducing charge carriers into the square layered lattice. While the average crystal symmetry and magnetic structure remain the same as in the parent compound, the addition of F results in an enhanced buckling of the $Fe(O/F)_2$ square plaquettes that is most likely topologically driven.

Oxyfluorides are of great interest due to their technological applications such as in light emitting diodes and as electrolytes in fuel cells and aqueous batteries.[1-4] Furthermore, the appearance of superconductivity upon fluorine doping in several systems including $Nd_2CuO_{4-x}F_x$,[5] $Sr_2CuO_2F_{2+\delta}$,[6] $LaO_{1-x}F_xFeAs$[7] and $WO_{3-x}F_x$[8] has motivated the search for new oxyfluorides with novel structures and functionalities.[9] To this end, attention has centred on two–dimensional lattices as they have become a platform from which emergent phenomena including massless Dirac fermions[10] and superconductivity[11] have been observed.

Recently the two-dimensional $SrFeO_2$,[12,13] a structural analogue of the superconducting $SrCuO_2$, has been synthesized by a topotactic method which is a low temperature synthesis route. The $SrCuO_2$-based materials with infinite layers of CuO_2 sheets become superconducting when charge carriers are introduced through rare earth ion doping.[11,14] However, the latter compounds are prepared under high temperature and pressure, and are metastable at ambient conditions.[11] In contrast, the moderate synthesis conditions of $SrFeO_2$ allow for better control of the reaction.[13] $SrFeO_2$ is an antiferromagnetic insulator with a Néel transition temperature of T_N ~ 473 K.[12] The presence of the very strong magnetic interactions and the high T_N are unusual for a two-dimensional system. Earlier neutron studies showed that the magnetic exchange coupling is sensitively influenced by localized modes involving transverse displacements of O and Fe, leading to buckling of the infinite sheets.[15] The buckling is enhanced by rising temperatures just as the Fe magnetic moment is reduced, implying a strong spin-lattice coupling.

The introduction of fluorine ions as a means to introducing electron carriers in the two-dimensional lattice of $SrFeO_2$ has not been previously explored and the purpose of the present work. The synthesis of $SrFeO_{2-x}F_x$, by combining two topotactic reactions, yields the first example of an infinite-layer oxyfluoride. Very recently, the layered structure of $Sr_3Co_2O_4Cl_2$, which consists of infinite sheets of CoO_2 and mixed anions, has been synthesized.[16] The Cl^{-1} anions are introduced during the parent compound $Sr_3Co_2O_5Cl_2$ synthesis however, and do not enter the CoO_2 planes. In contrast, the F^{-1} anions are introduced directly on the planes of $SrFeO_2$, and in this communication, the magnetic and structural properties with fluorine doping are presented.

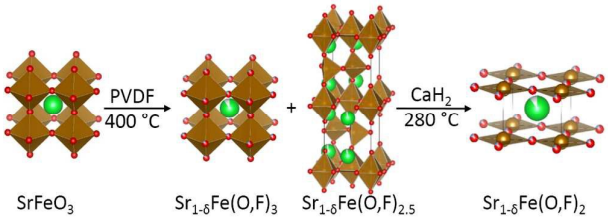

Figure 1. A schematic of the synthesis procedure of $Sr_{1-\delta}FeO_{2-x}F_x$.

The synthesis of the oxyfluoride $SrFeO_{2-x}F_x$ is outlined in Figure 1. $SrFeO_3$ is obtained by sintering $SrCO_3$ and Fe_2O_3 at 1000 °C for 24 hours. This step is repeated with intermediate grinding and re-pressing into pellets. The pure $SrFeO_3$ is ground with PVDF (polyvinylidene fluoride) in 1:0.1, 1:0.15, and 1:0.2 molar ratios, and pressed into pellets, in order to yield 20, 30, and 40 % of nominal F doping, respectively. The pellets are annealed under N_2 flow at 400 °C for 48 hours. The intermediate product consists of mostly the cubic $SrFe(O,F)_3$ and orthorhombic brownmillerite $SrFe(O,F)_{2.5}$ compounds along with a small amount of SrF_2 impurity (Figure S1).[17] The fluorinated cubic phase has an expanded unit cell in

[a] Department of Physics, University of Virginia, 382 McCormick Road, Charlottesville, VA 22904, USA.
[b] Spallation Neutron Source, Oak Ridge National Laboratory, Oak Ridge, TN 37831, USA.
[c] Mechanical, Aerospace and Biomedical Engineering, University of Tennessee Space Institute, Tullahoma, TN 37388, USA.
[d] Center for Laser Applications, University of Tennessee Space institute, Tullahoma, TN 37388, USA
† louca@virginia.edu
Electronic Supplementary Information (ESI) available: [structural details]. See DOI: 10.1039/x0xx00000x

ChemComm Accepted Manuscript

Please do not adjust margins

comparison to the non-fluorinated phase.[18-22] The sample is subsequently sealed with CaH_2 under Ar atmosphere and heated to 280 °C for 48 hours in a 3:2 weight ratio. The residual CaH_2 and the CaO byproducts are removed from the final reaction phase by washing them out with a solution of NH_4Cl/methanol. Neutron diffraction measurements were performed on the three nominal compositions of 20, 30 and 40 % as a function of temperature at the Neutron Powder Diffractometer (NPDF) of the Los Alamos National Laboratory. From the Rietveld refinement of the data, it is suggested that the fraction of the impurity phase, SrF_2, in the final product increases with the F doping level from 4.98, 8.46, to 10.90 %, respectively.

All fluorinated samples crystallize in the same symmetry as in $SrFeO_2$, with space group *P4/mmm* (see Figure 2 and Figure S3). With increasing doping, the *a*- and *c*-lattice parameters become smaller (Figure S2). The reduction of the a-lattice constant in the new phase in comparison to $SrFeO_2$ is most likely due to the inclusion of fluorine in the unit cell, while the decrease of the c-axis is most likely related to the presence of Sr vacancies in between the layers. The magnetic structure is determined to be antiferromagnetic with G-type ordering as shown in the inset of Figure 2, with a characteristic wave-vector of (1/2, 1/2, 1/2). The investigate whether or not fluorine is incorporated in the $SrFeO_2$ lattice, Mossbauer spectra using with a **Rh**^{57}Co source were collected on the nominal 40 % fluorine doped sample as a function of temperature. The results from three temperature measurements are shown in Figure 2(b). At 285 K, the values obtained for Fe^{2+} (red line) are in good agreement with those in Refs. [12] and [23] for $SrFeO_2$. In addition, a quadrupole doublet with a splitting ½e^{2}Qq of 2.39 mm/s, an isomer shift of δ = 1.24 mm/s and an intensity which is 20 % relative to the magnetic component of Fe^{2+} is observed. Typical values of the isomer shifts of the different valance states of Fe are given in Table S4. For Fe^{2+} in a fourfold square-planar coordination (as in Gillespite) the shift has been measured[24] to be 0.75 mm/s (when corrected for the **Pd**^{57}Co source), in good agreement with the value in Table S4[25,26,27]. A similar reduction for Fe^{+} would give a value δ = 1.25 mm/s which is consistent with the value δ = 1.24 mm/s found for the doublet in the current measurement for Fe^{1+}. At 6 K the Fe^{1+} doublet has split. It has a smaller field of about 279 kG (compared to 462 kG for Fe^{2+} at 6 K) and it has the same shift (1.24 mm/s) which indicates that it has become magnetic. The transition is not sharp and begins at around 20 K as seen in Figure S4. As the temperature is reduced to 100 K, a weak (18 %) hyperfine sextet is observed with a hyperfine field of 330 kG which is slightly stronger at 6 K. This is due to metallic iron which appears to be weakly bound as it has a low Debye-Waller factor at 285 K, suggesting that it is on the surface of the crystallites.

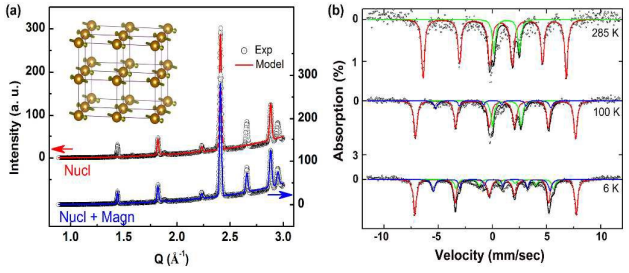

Figure 2. In (a), the diffraction pattern of $Sr_{0.891}FeO_{1.818}F_{0.182}$ at 10 K is shown. The magnetic structure is shown in the inset. The wRp and Rp are 0.110 and 0.084. In (b), the Mossbauer spectra at three temperatures show three lines, from Fe^{1+} (green), Fe^{2+} (red) and Fe^{3+} (blue).

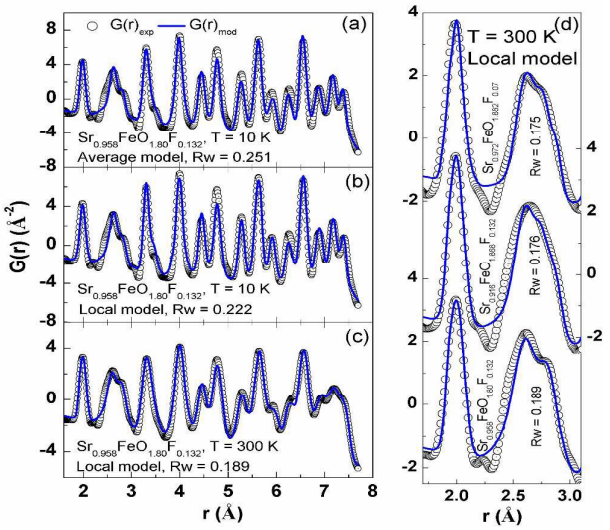

Figure 3. Comparison of the PDF with two models. In (a), the P4/mmm model (solid line) is compared with the data (symbols) for x = 0.132 at 10 K. In (b), the same data is compared with a local model. In (c), the same local model is extended to fit the data at 300 K. In (d), the local model is compared to the data of all three compositions. The goodness of fit is as indicated.

The diffraction data were further corrected for instrumental background and sample containment, and normalized by a vanadium standard. Absorption and multiple scattering corrections were applied as well. The structure function, S(Q), obtained from the diffraction data as a function of Q, the momentum transfer, was Fourier transformed to obtain the pair density function (PDF), G(r). The PDF is a real space representation of the atomic correlations.

In pure $SrFeO_2$, it was earlier shown that buckling of the FeO_2

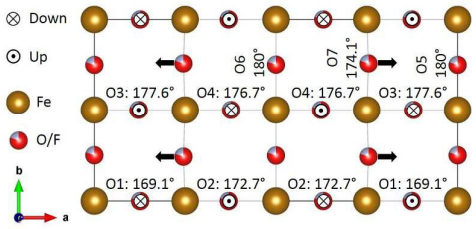

Figure 4. The motion of oxygen and fluorine is shown in the 2-dimensional plane at 300 K for $Sr_{0.958}FeO_{1.80}F_{0.132}$. The atoms represented in circles represent the up and down motion of O/F1, O/F2, O/F3 and O/F4 along the c-axis, while the arrows show the in-plane displacement of O/F7**.**

planes lowers the global *P4/mmm* symmetry.[15] The distortions, best described within the monoclinic *P2/m* symmetry, involve static displacements of oxygen and iron. The distortions become most significant above room temperature and continue through the magnetic transition of 473 K. Coupled with this distortion is the Fe-to-Fe magnetic interactions. Three magnetic coupling constants are present due to direct exchange and superexchange interactions. Distorions of the O and Fe sublattices weaken the interactions, driving the system to the paramagnetic state. What happens to the square plaquette with the introduction of F?

ChemComm Accepted Manuscript

This journal is © The Royal Society of Chemistry 2015

Shown in Figure 3 are the PDF's corresponding to the local structure of the three fluorine compositions. In Figure 3(a), the data for $Sr_{0.958}FeO_{1.80}F_{0.132}$ (symbols) is compared to a model calculated based on the atomic coordinates and unit cell dimensions of the P4/mmm crystal cell (solid line). The average structure model provides a very good fit to the data at 10 K (Fig. 3a). Some differences are observed, particularly with the second and fifth correlations that suggests that the local symmetry is lower. The data is fit to a local model where the O/F atoms are displaced as shown below (Fig. 3b) The differences become quite pronounced as the temperature rises and displacements become larger (Fig. 3c). These differences are observed in the other compositions as well. While the first peak is almost composition independent, subsequent peaks exhibit noticeable changes, attributed to an enhanced in-plane buckling as will be discussed below (see Figure 3(d)).

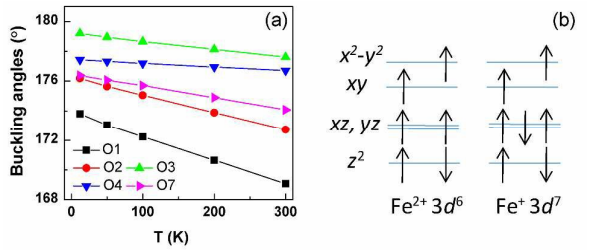

Figure 5. (a) The temperature dependence of the buckling angles assoicated with sites 1, 2, 3, 4 and 7 in $Sr_{0.958}FeO_{1.80}F_{0.132}$. (b) The schematic electronic levels for Fe^{2+} and Fe^{+}.

To reproduce the local atomic arrangement, the fluorinated lattice is distorted, where the onset temperature for the distortions is significantly lower than what was previously observed in $SrFeO_2$. In the $Sr_{0.958}FeO_{1.80}F_{0.132}$, the FeO_2 plane is distorted as shown in Figure 4 where the O/F displacements are out of phase along the *b* axis. The displacements alternate between large (O/F)1 and (O/F)2 and small (O/F)3 and (O/F)4). The structural details are provided in Table S2. By 300 K, the corresponding displacements are 0.1910, 0.1285, 0.076, and 0.059 Å for (O/F)1, (O/F)2, (O/F)3, and (O/F)4, respectively. The local model corresponding to the proposed distortion pattern of Figure 4 is best represented by the P2/m monoclinic symmetry and is compared to the data of x = 0.182 at 10 K (Figure 3(b)) and 300 K (Figure 3(c)). It can clearly be seen that the fit is quite good at both temperatures. Note that in this model, Fe is not displaced.

The undulations resulting from the motion of O/F reduce the bond angle from the ideal 180° between Fe and O/F. In Figure 5a, the buckling angle between five O/F sites in the monoclinic symmetry and Fe is plotted as a function of temperature for $Sr_{0.958}FeO_{1.80}F_{0.132}$. The angle is continuously reduced with both temperature and composition. With F doping, the FeO_2 square plaquettes are significantly buckled mostly due to the c-axis displacements of O/F at sites 1 and 2. Shown in Figure 5b is a schematic of the electronic level diagram of Fe^{2+} and Fe^{1+} in the square planar crystal field geometry. In this configuration, no Jahn-Teller distortion is expected and the lowest orbitals are the d_{z2-r2} and d_{xz} and d_{yz}. In Fe^{1+} with the $3d^7$ configuration, the extra electron can occupy any one of the $3d_{xy}$, $3d_{yz}$, or $3d_{xz}$ orbitals, reducing the total moment S from 2 to 3/2, in agreement with the reduction of the observed moment.

Comparison of $SrFeO_2$ to $LaNiO_2$ which are isostructural to $SrCuO_2$, the parent phase of the high-T_c superconductors is of interest here. $LaNiO_2$ was first synthesized by reducing $LaNiO_3$ with H_2 at 300 °C in 1983, before the discovery of high-Tc superconductors.[28,29] $LaNiO_3$ was later transformed to $LaNiO_2$ using NaH at 200 °C.[30] It is weakly insulating with no magnetic order. However, $SrFeO_2$ is a strong localized antiferromagnet with T_N around 473 K and a magnetic moment of 3.6 μ_B. Thus, it is interesting to introduce F into the $LaNiO_2$ lattice. Since $LaNiO_3$ is not stable at high temperatures in air and only survives in high O_2 pressure, XeF_2 can be a choice for fluorination, by which the reaction can take place at around 100 °C.[31,32]

To summarize, infinite-layer oxyfluorides $SrFeO_{2-x}F_x$ have been synthesized by combining topotactic fluorination with PVDF and reduction with CaH_2. This is the first example of an oxyfluoride with an infinite-layer structure. In $SrFeO_2$, the iron moment is localized and the system is insulating. Fluorine doping does not drive the system to an insulator-metal phase boundary in spite of the introduction of charge carriers, indicating that $SrFe(O,F)_2$ is located far away from the insulating-metal boundary. Even though the crystal and magnetic structures remain unchanged, locally the lattice undergoes significant distortions with doping. This synthesis technique may be useful to explore possible routes to creating two-dimensional lattices that might exhibit superconductivity like in $SrCuO_2$ and $LaNiO_2$.

Notes and references

This work has been supported by Department of Energy, Grant number DE-FG02-01ER45927.

1 Y. Tsujimoto, K. Yamaura and E. Takayama-Muromachi, Appl. Sci. 2012, **2**, 206.
2 C. Zhu, J. Wang, M. Zhang, X. Ren, J. Shen and Y. Yue, J. Am. Ceram. Soc. 2014, **97**, 854.
3 E. Sullivan and T. Vogt, ECS J. Solid State Sci. Technol. 2013, **2**, R3088.
4 G. G. Amatucci and N. Pereira, J. Fluor. Chem. 2007, **128**, 243 (and references therein).
5 A. C. W. P. James, S. M. Zahurak and D. W. Murphy, Nature 1989, **338**, 240.
6 M. Al-Mamouri, P. P. Edwards, C. Greaves and M. Slaski, Nature 1994, **368**, 382.
7 Y. Kamihara, T. Watanabe, M. Hirano and H. Hosono, J. Am. Chem. Soc. 2008, **130**, 3296.
8 D. Hirai, E. Climent-Pascual and R. J. Cava, Phys. Rev. B 2011, **84**,174519.
9 B. Li, Y. N. Chen, H. Wang, W. Liang, G. Y. Liu, W. J. Ren, C. F. Li, Z. Q. Liu, G. H. Rao, C. Q. Jin and Z. D. Zhang, Chem. Commun. 2014, **50**, 799.
10 K. S. Novoselov, A. K. Geim, S. V. Morozov, D. Jiang, M. I. Katsnelson, I. V. Grigorieva, S. V. Dubonos and A. A. Firsov, Nature 2005, **438**, 197.
11 T. Siegrist, S. M. Zahurak, D. W. Murphy and R. S. Roth, Nature 1988, **334**, 231.
12 Y. Tsujimoto, C. Tassel, N. Hayashi, T. Watanabe, H. Kageyama, K. Yoshimura, M. Takano, M. Ceretti, C. Ritter and W. Paulus, Nature 2007, **450**, 1062.
13 C. Tassel and H. Kageyama, Chem. Soc. Rev. 2012, **41**, 2025.
14 M. G. Smith, A. Manthiram, J. Zhou, J. B. Goodenough and J. T. Markert, Nature 1991, **351**, 549.
15 K. Horigane, A. Llobet and D. Louca, Phys. Rev. Lett. 2014, **112**, 097001.
16 F. D. Romero, L. Coyle and M. A. Hayward, J. Am. Chem. Soc. 2012, **134**, 15946.
17 E. Sullivan, and C. Greaves, Mater. Res. Bull. 2012, **47**, 2541.

ChemComm Accepted Manuscript

18 C. K. Blakely, J. D. Davis, S. R. Bruno, S. K. Kraemer, M. Z. Zhu, X. L. Ke, W. L. Bi, E. E. Alp and V. V. Poltavets, J. Fluor. Chem. 2014, **159**, 8.
19 C. M. Thompson, C. K. Blakely, R. Flacau, J. E. Greedan and V. V. Poltavets, J. Solid State Chem. 2014, **219**, 173.
20 O. Clemens, R. Haberkorn, P. R. Slater, and H. P. Beck, Solid State Sci. 2010, **12**, 1455.
21 O. Clemens, F. J. Berry, J. Bauer, A. J. Wright, K. S. Knight and P. R. Slater, J. Solid State Chem. 2013, **198**, 262.
22 O. Clemens, F. J. Berry, J. Bauer, A. J. Wright, K. S. Knight and P. R. Slater, J. Solid State Chem. 2013, **203**, 218.
23 N. Hayashi, H. Kageyama, Y. Tsujimoto, T. Watenabe, S. Muranaka, T. Ono, S. Nasu, Y. Ajiro, K. Yoshimura and M.Takano, J. Phys. Soc. Japan 2010, **79**, 123709.
24 M.G. Clark, G.M. Bancroft and A.J. Stone, J. Chem. Phys. 1967, **47**, 4260.
25 J. Chappert, R.B. Frankel, A. Misetich and N.A. Blum, Phys. Rev. 1969, **179,** 578.
26 C. Garcin, A. Gerard and P. Imbert, J. Phys. Chem. Solids 1990, **51,** 1281.
27 A.P. Khomyakov, V.V. Korovushkin, Yu. D. Perfiliev and V.M. Cherepanov, Phys. Chem. Minerals 2010, **37.** 543.
28 J. M. Greneche, V. Venkatesan, R. Suryanarayanan, J. M. D. Coey, Phys. Rev. B 2011, **63**, 174403.
29 M. T. Mock, C. V. Popescu, G. P. A. Yap, W. G. Dougherty, C. G. Riordan, Inorg. Chem. 2008, **47**, 1889.
30 M. Crespin, P. Levitz and L. Gatineau, J. Chem. Soc. Faraday Trans. 1983, **2**, 1181.
31 P. Levitz, M. Crespin and L. Gatineau, J. Chem. Soc. Faraday Trans. 1983, **2**, 1195.
32 M. A. Hayward, M. A. Green, M. J. Rosseinsky and J. Sloan, J. Am. Chem. Soc. 1991, **121**, 8843.

ChemComm Accepted Manuscript

This journal is © The Royal Society of Chemistry 2015